






Article

M(II)Al₄ Type Layered Double Hydroxides—Preparation Using Mechanochemical Route, Structural Characterization and Catalytic Application

Márton Szabados ^{1,2}, Adél Anna Ádám ², Zsolt Kása ², Kornélia Baán ³, Róbert Mucsi ³, András Sági ³, Zoltán Kónya ^{3,4}, Ákos Kukovecz ³ and Pál Sipos ^{2,5,*}

¹ Department of Organic Chemistry, University of Szeged, Dóm tér 8, H-6720 Szeged, Hungary; szabados.marton@chem.u-szeged.hu

² Material and Solution Structure Research Group, Institute of Chemistry, University of Szeged, Aradi Vértanúk tere 1, H-6720 Szeged, Hungary; adeladam@chem.u-szeged.hu (A.A.Á.); kasa.zsolt@chem.u-szeged.hu (Z.K.)

³ Department of Applied and Environmental Chemistry, University of Szeged, Rerrich B. tér 1, H-6720 Szeged, Hungary; kornelia.baan@chem.u-szeged.hu (K.B.); muule93@gmail.com (R.M.); sapia@chem.u-szeged.hu (A.S.); konya@chem.u-szeged.hu (Z.K.); kakos@chem.u-szeged.hu (Á.K.)

⁴ MTA-SZTE Reaction Kinetics and Surface Chemistry Research Group, Rerrich B tér 1, H-6720 Szeged, Hungary

⁵ Department of Inorganic and Analytical Chemistry, University of Szeged, Dóm tér 7, H-6720 Szeged, Hungary

* Correspondence: sipos@chem.u-szeged.hu



Citation: Szabados, M.; Ádám, A.A.; Kása, Z.; Baán, K.; Mucsi, R.; Sági, A.; Kónya, Z.; Kukovecz, Á.; Sipos, P. M(II)Al₄ Type Layered Double Hydroxides—Preparation Using Mechanochemical Route, Structural Characterization and Catalytic Application. *Materials* **2021**, *14*, 4880. <https://doi.org/10.3390/ma14174880>

Academic Editor: Halina Kaczmarek

Received: 9 August 2021

Accepted: 25 August 2021

Published: 27 August 2021

Publisher's Note: MDPI stays neutral with regard to jurisdictional claims in published maps and institutional affiliations.



Copyright: © 2021 by the authors. Licensee MDPI, Basel, Switzerland. This article is an open access article distributed under the terms and conditions of the Creative Commons Attribution (CC BY) license (<https://creativecommons.org/licenses/by/4.0/>).

Abstract: The synthesis of the copper-poor and aluminum-rich layered double hydroxides (LDHs) of the CuAl₄ type was optimized in detail in this work, by applying an intense mechanochemical treatment to activate the gibbsite starting reagent. The phase-pure forms of these LDHs were prepared for the first time; using copper nitrate and perchlorate salts during the syntheses turned out to be the key to avoiding the formation of copper hydroxide sideproducts. Based on the use of the optimized syntheses parameters, the preparation of layered triple and multiple hydroxides was also attempted using Ni(II), Co(II), Zn(II) and even Mg(II) ions. These studies let us identify the relative positions of the incorporating cations in the well-known selectivity series as Ni²⁺ >> Cu²⁺ >> Zn²⁺ > Co²⁺ >> Mg²⁺. The solids formed were characterized by using powder X-ray diffractometry, UV–Vis diffuse reflectance spectroscopy, Fourier-transform infrared spectroscopy, thermogravimetric analysis and scanning electron microscopy. The catalytic potential of the samples was investigated in carbon monoxide oxidation reactions at atmospheric pressure, supported by an in situ diffuse reflectance infrared spectroscopy probe. All solids proved to be active and the combination of the nickel and cobalt incorporation (which resulted in a NiCoAl₈ layered triple hydroxide) brought outstanding benefits regarding low-temperature oxidation and increased carbon monoxide conversion values.

Keywords: gibbsite intercalation; copper- and magnesium-poor layered double hydroxides; mechanochemistry; catalytic carbon monoxide oxidation

1. Introduction

Layered double hydroxides (LDH) belong to a group of anionic clay-type materials possessing a CdI₂-type structure. Due to the chemical diversity offered by variability in the composition of the interlamellar galleries and layers, they can be finely tuned to numerous applications, from healthcare [1] to agriculture [2] and the polymer industry [3], just to mention a few. Perhaps the most promising research field of the pristine and heat-treated derivatives of LDHs is their application as catalysts. The majority of LDHs have an intrinsically basic character and the cationic components, with alternating oxidation states, serve as redox centers. Hence, these compounds are commonly employed in transesterification [4], Michael addition [5], or even in photochemical transformations [6]. The following formula

is used for the description of the LDHs: $[M^{2+}_{1-x}M^{3+}_x(OH)_2]^{x+}[A^{n-}_{x/n} \cdot mH_2O]^{x-}$, where M^{2+} and M^{3+} are the di- and trivalent metal ions, respectively, while A^{n-} stands for the interlamellar anions with a charge of n , and $x = M^{3+}/[M^{2+} + M^{3+}]$ [7]. The formation of their framework can be deduced in two ways, depending on the value of x . When $x \leq 0.5$, the LDHs can formally be derived from the brucite-like $(Mg(OH)_2)$ layered divalent metal hydroxides (with $M^{2+} = Mg^{2+}, Ca^{2+}, Ni^{2+}, Co^{2+}, Cu^{2+}, Zn^{2+}$, etc.) via the isomorphous substitution of divalent cations with trivalent ones (e.g., $Al^{3+}, Cr^{3+}, Fe^{3+}$, etc.). Thus, in the layers, a positive charge is built up and (hydrated) anions intercalate to compensate for the charge of the layer. The preference of intercalating various inorganic anions follows the lyotropic series of $CO_3^{2-} \gg SO_4^{2-} \gg OH^- > F^- > Cl^- > Br^- > NO_3^- > I^- \approx ClO_4^-$, which is mainly controlled by the size and the strength of the electrostatic interaction [8,9].

At higher x values, the incorporation of divalent ions (or, e.g., the monovalent Li^+) also results in the formation of an LDH-type structure; however, so far, only aluminum trihydroxide was found to be suitable for generating these M(III)-rich and, thus, M(I)-, M(II)-poor layered double hydroxides (with the following general formula: $[M(I)_2/M(II) - M(III)_4(OH)_{12}]^{2+}[A^{n-}_{2/n} \cdot mH_2O]^{2-}$). The key is the structural similarity of their frameworks to that of brucite, but appearing here with vacant octahedral holes in which the extraneous metal cations could incorporate, resulting in positively charged layers. This creates the need for the formation of the anion-containing interlamellar galleries. These LDHs have excellent ion-exchange properties [10] and modified anion exchange capability, with a preference for the tetrahedral anions and, hence, a lower affinity for the CO_3^{2-} anions compared to that of the more conventional ($x \leq 0.5$) LDHs [11,12].

The success of the incorporation of extraneous metal ions and the generation of the LDH phase is limited by a variety of factors. These are the ionic radii and the solvation energies of the metal cations [11], the solubility of the metal salts used, and the quality of the interlamellar anions with regard to their position in the lyotropic series. Therefore, the incorporation of the Li^+ (having a suitable ionic radius, good solubility in water, and relatively low hydration enthalpy), and the formation of $LiAl_2$ -LDH in the direct reaction of the aluminum hydroxide and various lithium salts resulted in the occupation of all the vacant holes and the intercalation of numerous inorganic anions: $X^- = Cl^-, Br^-, NO_3^-, SO_4^{2-}, OH^-$ and CO_3^{2-} [13,14]. For the incorporation of M(II) cations, several studies were reported in the last two decades; however, until now, the successful incorporation of $Mg^{2+}, Co^{2+}, Ni^{2+}, Cu^{2+}$ and Zn^{2+} meant the occupation of half of the octahedral holes, resulting in $M(II)Al_4$ -LDHs. For this, the use of harsh synthesis conditions, that is, concentrated (2–10 M) metal NO_3^-, SO_4^{2-} and Cl^- salt solutions, hydrothermal conditions (120–150 °C reaction temperature), and long reaction times (24–72 h) were necessary [15–18]. Moreover, so far, the synthesis of the copper-containing variants in a phase-pure form was found to be impossible, due to the concomitant formation of copper hydroxide impurities. Hence, the position of the Cu(II) in the selectivity series of cation incorporation ($Li^+ \gg Ni^{2+} \gg Co^{2+} \approx Zn^{2+}$) was unknown [19]. The case of $MgAl_4$ -LDHs is somewhat similar, in the sense that preparation was found to be rather complicated [16,17].

In the synthesis procedures, the application of mechanochemical pretreatment is not a necessity [11–14,16,18,20]; however, in several cases, mechanically activated aluminum hydroxide particles were used for obtaining these LDHs [10,15,17,19,21]. Recently, a large number of simple-to-set-up, moderately priced instruments with specific operating characteristics have become commercially available, making it possible to carry out various mechanochemical treatments for the preparation of well-known [22] as well as unique LDHs [23]. In our recent work, it was demonstrated that high-energy milling could induce a unique polymorph transformation of $Al(OH)_3$ and facilitate the generation of LDHs [24].

Therefore, our aim was to explore the possibility of synthesizing phase-pure copper-containing aluminum-rich layered double hydroxides of a $CuAl_4$ type. Based on the knowledge gained, the same type of synthesis was attempted, using multiple metal ions (the parallel incorporation of Mg(II), Ni(II), Co(II) and Zn(II) ions to gain layered triple and multiple hydroxides) using intense mechanochemical pretreatment. The influence of the

counter anions of the starting copper salts on the synthesis and catalytic activities of the as-prepared materials were also explored in catalytic carbon monoxide oxidation.

2. Materials and Methods

2.1. Materials

The nickel, copper and magnesium salts ($\text{Ni}(\text{NO}_3)_2 \cdot 6\text{H}_2\text{O}$, $\text{Ni}(\text{ClO}_4)_2 \cdot 6\text{H}_2\text{O}$, $\text{Cu}(\text{NO}_3)_2 \cdot 3\text{H}_2\text{O}$, $\text{CuCl}_2 \cdot 2\text{H}_2\text{O}$, CuBr_2 , $\text{Cu}(\text{ClO}_4)_2 \cdot 6\text{H}_2\text{O}$, $\text{Mg}(\text{NO}_3)_2 \cdot 6\text{H}_2\text{O}$, and $\text{Mg}(\text{ClO}_4)_2 \cdot 6\text{H}_2\text{O}$) were purchased from Merck (St. Louis, MO, USA), while the zinc and cobalt salts ($\text{Zn}(\text{NO}_3)_2 \cdot 6\text{H}_2\text{O}$, $\text{Zn}(\text{ClO}_4)_2 \cdot 6\text{H}_2\text{O}$, $\text{Co}(\text{NO}_3)_2 \cdot 6\text{H}_2\text{O}$, $\text{Co}(\text{ClO}_4)_2 \cdot 6\text{H}_2\text{O}$) were provided by the Alfa Aesar (Kandel, Germany). Anhydrous $\text{Al}(\text{OH})_3$ (gibbsite) was received from Reanal Private (Budapest, Hungary). The chemicals were of 99%+ purity and were used without additional purification.

2.2. Mechanical Pretreatment of Gibbsite

For the pre-milling steps, a Retsch MM 400 mixer mill (Retsch GmbH, Haan, Germany), equipped with two stainless steel grinding balls of $\sim 8.2 \text{ cm}^3$ (25 mm diameter) and grinding jars (50 cm^3 inner volume), were used. In all cases, the dry-milling of the $\text{Al}(\text{OH})_3$ was executed at 12 Hz grinding frequency and 100 ball/sample mass ratio. (We would like to highlight here that the specific structural changes caused by a vibration/mixer mill are in part different from those that evolve in a rolling or planetary ball mill during its circular motion [25]; here, the jars pass in radial oscillations along the horizontal axis and, inside, the balls collide with the rounded ends of the jars, resulting in intense collisions of short duration.)

2.3. Preparation of the Magnesium-, Copper-, Nickel-, Cobalt- and Zinc-Poor $M(\text{II})\text{Al}_4\text{-LDHs}$

The first step of each synthesis was the mechanochemical pretreatment of aluminum trihydroxide. In our recent work, it was shown that 4 h of grinding time and 3 days of impregnation were the optimal conditions for the preparation of phase-pure $\text{NiAl}_4\text{-LDHs}$ [24]. In this study, the preparation of cobalt, copper, zinc and magnesium salts required an increase of milling duration of up to 6–12 h, and 4 days of impregnation time. In all cases, 100 mg of activated $\text{Al}(\text{OH})_3$ solid was placed in a glass tube with the metal salt dissolved in 5 cm^3 distilled water. The initial $M(\text{II})\text{:Al}$ ratio was systematically varied in a wide range to test its influence on the success of LDH preparation. The synthesis of the layered triple (LTHs) and multiple hydroxides (LMHs) was executed by the addition of a mixture of the required metal salts to the gibbsite powder. The obtained suspensions were stirred at $90 \text{ }^\circ\text{C}$ with a 1000 rpm stirring rate under an air atmosphere. The samples were collected on filters with $0.45 \text{ }\mu\text{m}$ pore size, washed with distilled water (200–1000 mL) several times (the protocol depended on the concentration of the impregnating solution), and were dried at $80 \text{ }^\circ\text{C}$ overnight.

2.4. Carbon Monoxide Oxidation in a Continuous Flow Reactor

The catalytic reactions were performed in a fixed-bed continuous-flow reactor (University of Szeged, Szeged, Hungary) (8 mm internal diameter, 200 mm length), externally heated with a thermocouple between 100 and $700 \text{ }^\circ\text{C}$; $100 \pm 2 \text{ mg}$ samples were weighed and placed between quartz wool plugs. At atmospheric pressure, discontinuous heating was used and the reactor was heated up at a $10 \text{ }^\circ\text{C}/\text{min}$ rate; the targeted temperatures were held for 25 min, and the gas samplings were carried out in the seventh minute. Prior to the measurements being taken, the solids were degassed at $110 \text{ }^\circ\text{C}$ for 2 h in an Ar atmosphere. The flow rate and composition of the reacting gas mixture were as follows: carbon monoxide— $4 \text{ cm}^3/\text{min}$, oxygen— $10 \text{ cm}^3/\text{min}$, and argon— $46 \text{ cm}^3/\text{min}$. To avoid any condensation, the tubes delivering the gases were also externally heated between the reactor and the HP 5890 gas chromatograph (Hewlett-Packard, Waldbronn, Germany) equipped with a Porapak Q packed column for thermal conductivity detection. The analysis of the composition of the products was performed using $120 \text{ }^\circ\text{C}$ injections and a $250 \text{ }^\circ\text{C}$

detector temperature; the oven was heated from 45 °C (with a 6-min hold) up to 180 °C, with a 4-min hold and 10 °C/min heating rate.

2.5. Methods of Structural Characterization

The main method used to monitor the success of the synthesis and the obtained phase compositions was powder X-ray diffractometry, using a Rigaku Miniflex II diffractometer (Rigaku Corporation, Tokyo, Japan), equipped with a scintillation detector and a Ni foil $K\beta$ filter (operating at 30 kV and 15 mA). The normalized XRD patterns were registered in the $\theta = 5\text{--}80^\circ$ range using $\text{CuK}\alpha$ ($\lambda = 1.5418 \text{ \AA}$) radiation, with a $4^\circ/\text{min}$ scan speed in continuous mode and a step width of $0.02^\circ 2\theta$. The average crystallite sizes of LDHs (coherently scattering domain sizes—the crystallite thicknesses from layers connected to each other in the c -axis direction of the platelets) were estimated from the full width at half-maximum (FWHM) of the first reflections, applying Gaussian distribution and the Scherrer equation with a shape factor of 0.9. The reflections of the patterns were identified with the help of the JCPDS-ICDD (Joint Committee of Powder Diffraction Standards—International Centre for Diffraction Data) database.

To investigate the structural properties of the LDHs, Fourier-transform infrared (FT-IR) spectra were registered on a JASCO FT/IR-4700 spectrophotometer (Kyoto, Japan), accumulating 256 scans at 4 cm^{-1} resolution with a ZnSe ATR attachment and DTGS detector. The normalized spectra were obtained in the $4000\text{--}600 \text{ cm}^{-1}$ wavenumber range.

The metal content of the samples was analyzed by an Agilent 7900 ICP-MS (Agilent Technologies, Santa Carla, CA, USA) (inductively coupled plasma mass spectrometry) spectrometer using ICP multielement standard solution IV (Certipur). The solids were dissolved in hydrochloric acid with the aid of microwave digestion.

The optical properties of the LDHs were probed by diffuse reflectance spectroscopy (DRS) with an Ocean Optics USB4000 spectrometer (Ocean Insight, Duiven, Netherlands) and DH-2000-BAL light source. As the white reference, BaSO_4 was used in the 225–890 nm wavelength range. For the transformation of the reflectance spectra into absorption, the Schuster–Kubelka–Munk function was used, while the optical energy gaps were determined by the extrapolation of the straight section of the modified Schuster–Kubelka–Munk function, as plotted vs. the energy of the incident light (Tauc-plot).

To characterize the thermal behavior of the materials, thermogravimetric and differential thermal analysis (TGA and DTA) were performed in the 40–800 °C temperature range by applying a Netzsch STA 409 PC Luxx derivatograph (Netzsch Holding, Selb, Germany), using a constant flow (60 mL/min) of synthetic air and a $10^\circ\text{C}/\text{min}$ heating rate. The samples were taken into high-purity alpha-alumina crucibles, and 40–50 mg solids were employed.

The morphology of the materials was visualized by a Hitachi S-4700 scanning electron microscope (SEM) (Hitachi Ltd, Tokyo, Japan) at various acceleration voltages. Onto the surface of solids, a few nanometers of a conductive gold film were sublimed to avoid the electrostatic charging of the particles. Elemental analysis was carried out by energy-dispersive X-ray spectroscopy (Roentec AG, Berlin, Germany) measurements (EDXS, Röntec QX2 spectrometer installed with a Be window and coupled to the SEM).

The in situ diffuse reflectance infrared Fourier-transform spectroscopy (DRIFTS) measurements were executed using an Agilent Cary-670 FTIR spectrometer (Agilent Technologies, Santa Carla, CA, USA) equipped with a Harrick Praying Mantis diffuse reflectance cell with two BaF_2 windows. The samples were warmed linearly up to 550 °C with a $20^\circ\text{C}/\text{min}$ heating rate. The spectra were registered in the $4000\text{--}800 \text{ cm}^{-1}$ wavenumber range, accumulating 32 scans at 2 cm^{-1} resolution. The purging gas was He and the mixture of the CO and He gas (10 and 90 vol %, $40 \text{ cm}^3/\text{min}$) was introduced in the cell. The spectra of the pristine catalysts were used as background.

3. Results and Discussion

3.1. Optimization of the Synthesis Parameters for the Preparation of $\text{CuAl}_4\text{-LDHs}$

First, the quality of the copper salt starting reagents was systematically varied, in order to investigate their influence on the success of the preparation of $\text{CuAl}_4\text{-X}^{n-}\text{-LDHs}$ (X^{n-} is the anion of the copper salt). The use of all salts resulted in the formation of the corresponding LDHs (the identification of the reflections was carried out according to the literature [16,19]). The variation of the basal spacing (that is, the sum of the thickness of a layer, plus the interlayer distance) was found to depend on the size of the interlamellar anion, X^{n-} . The smallest size was obtained for $\text{CuAl}_4\text{-Cl}^-\text{-LDH}$ (7.5 Å, Figure S1; hereafter, “S” refers to information found in the Supporting Information), while the largest was observed for $\text{CuAl}_4\text{-ClO}_4^-\text{-LDH}$ (9.0 Å, Figure 1). When chloride and bromide salts were used, the formation of various side products was observed; next to the $\text{CuAl}_4\text{-Cl}^-\text{-LDHs}$, the reflections of gibbsite (designated as $\gamma\text{-Al(OH)}_3$ —JCPDS#70-2038) and the tribasic copper chloride ($\text{Cu}_2(\text{OH})_3\text{Cl}$, JCPDS#25-1427) were permanently present (Figure S1). For the $\text{CuAl}_4\text{-Br}^-\text{-LDHs}$, the formation of dicopper bromide trihydroxide (JCPDS#74-1652) and the presence of an aluminum oxide bromide ($\text{Al}_3\text{O}_4\text{Br}$, JCPDS#17-0695) phase was registered (Figure S2). For both LDHs, the amount of the side products could be decreased significantly by using a minimal excess of the copper salt reagents (Cu:Al molar ratio of 3.0–3.5).

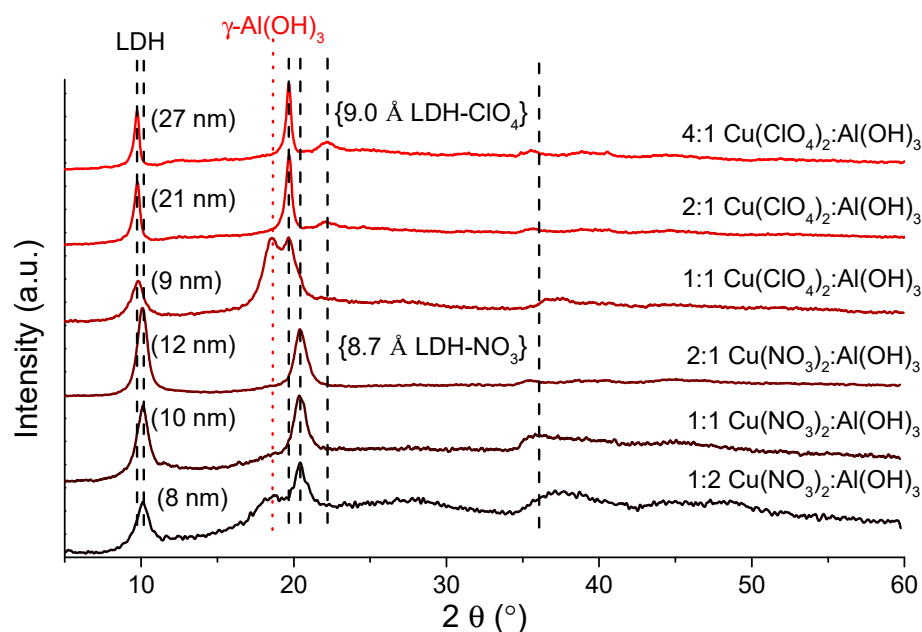


Figure 1. XRD patterns of the $\text{CuAl}_4\text{-X}^{n-}\text{-LDHs}$, formed with various X^{n-} interlayer anions. The initial Cu:Al molar ratio is shown to the right side of the XRD patterns; crystallite thicknesses are denoted next to the first reflection. Reaction conditions: 6 h pre-milling, 96 h stirring, 90 °C reaction temperature. The basal spacings in two representative cases are shown in curly brackets.

The preparation of nitrate- and perchlorate-containing LDHs was more favored; applying a suitable amount of the starting reagents (1:1 Cu:Al molar ratio for nitrate, and 2:1 Cu:Al molar ratio for perchlorate salts) resulted in the complete disappearance of the gibbsite phase and the formation of $\text{CuAl}_4\text{-NO}_3^-\text{-LDH}$ and $\text{CuAl}_4\text{-ClO}_4^-\text{-LDH}$, respectively (Figure 1). There were no reflections corresponding to possible impurities and the elemental analysis revealed, commonly, molar ratios close to 1:4 of Cu:Al, indicating that the amorphous gibbsite starting reagent was present only in minute amounts. Using the optimal synthesis conditions, the baseline shift (stemming partially from the disorders in the amorphous phases) could be decreased significantly (from 40–60 to 4–7 wt % amorphous phase content). The increase of the initial Cu:Al molar ratio facilitated the formation of

thicker LDHs; the intensity of the reflections increased and split at around 20 and 22° 2 θ for the CuAl₄-ClO₄⁻-LDH, which is a common phenomenon. This effect was already observed for LiAl₂- [26], ZnAl₄-LDHs [27] and, in our recent work, for NiAl₄-ClO₄⁻-LDH and for NiAl₄-NH₂SO₃⁻-LDH [24].

The FT-IR of the solids also verified the formation of phase-pure CuAl₄-Xⁿ⁻-LDHs. All the vibration bands observed could be clearly attributed to the characteristic vibrations of the aluminum-rich layered double hydroxides (Figure S3). The broad bands around 3500 cm⁻¹ can be connected to the stretching vibration of the network of OH groups in the hydroxide layers. The weak band at 1630 cm⁻¹ corresponds to the bending vibration of the interlamellar water molecules. Finally, the deformation and translation modes of the Al-OH moieties were registered under 1000 cm⁻¹ [28,29]. The weak ν_1 (1050 cm⁻¹) and ν_2 (820 cm⁻¹), and the strong ν_3 vibrations (1350 cm⁻¹) were recorded for the nitrate interlamellar molecules, and the ν_3 and ν_4 mode of the perchlorate anions could readily be observed at 1085 and 620 cm⁻¹, respectively, for the corresponding LDHs [30].

3.2. Preparation of Layered Triple- and Multiple Hydroxide Systems

The synthesis of the phase-pure CuAl₄-Xⁿ⁻-LDHs guided us to carry on the research started by Williams et al., in which the co-incorporation of M(II) ions was attempted, with the aim of establishing a preference order for the building of various metal ions into the gibbsite structure [19]. In our case, first, the NiCuAl-NO₃⁻-LTHs were studied in detail. It can be seen from the data shown in Table 1 that the ratio of the incorporated metal ions can be fine-tuned by varying the initial molar ratio of the starting nickel and copper nitrate salts. However, the variation of the added amounts of the nickel salt proved to be beneficial, in the sense that the decreasing Ni:Cu molar ratio did not result in the appearance of the reflections that are characteristic of dicopper nitrate trihydroxide (JCPDS#75-1779) impurities (Figures S4 and S5). The SEM-EDXS analysis (not shown) proved that the two cations are not segregated, verifying that these are present as a molecular level mixture—similar observations were made by Williams et al. [19]. The XRD patterns of the LTHs and their basal spacing values were practically identical to those obtained for the CuAl₄-NO₃⁻-LDHs. Interestingly, a clear correlation was observed between the decrease in the initial nickel content and the crystallite thicknesses, while the intensity of the second (0021) reflections remained largely unaltered (Figure S4).

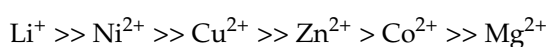
When working with cobalt, zinc and magnesium ions, it was necessary to know the optimal synthesis parameters leading to phase-pure LDHs. As expected, these cations are found at the end of the preference order, and the preparation of CoAl₄- and ZnAl₄-LDHs required large excess of the nitrate salt reagents; that is, 4:1 initial Co/Zn:Al molar ratios (Figure S6). For MgAl₄-NO₃⁻-LDH synthesis, as was more or less expected, the use of an even larger (Mg:Al = 32:1) molar ratio and an increase in the pre-milling time proved to be necessary (Figure S7). Using lower concentrations of the above M(II) ions, the conversion of the starting gibbsite into its dehydrated (boehmite, AlO(OH) JCPDS#83-2384) and polymorph (bayerite, as α -Al(OH)₃ JCPDS#83-2256) forms was recorded. Based on these observations, for the synthesis of the CoZnAl-, MgCoAl- and MgZnAl-LTHs and the MgCoZnAl-LMH, 4:4:1 and 4:4:4:1 initial molar ratios were employed, respectively, to prepare phase-pure LTH and LMH systems.

Table 1. The molar ratios of the incorporated metal ions into the gibbsite structure; the initial and the measured values in the formed LTHs/LMHs, and their direct and indirect optical band gap values.

| Samples (LDH-NO ₃) | Initial Molar Ratios ¹ | | | | | Measured Molar Ratios | | | | | Direct Band Gap (eV) | Indirect Band Gap (eV) |
|-----------------------------------|-----------------------------------|-------|----|----|----|-----------------------|-------|-------|-------|-------|-------------------------|---------------------------|
| | Mg | Ni | Co | Cu | Zn | Mg | Ni | Co | Cu | Zn | | |
| NiCu-Al | - | 0.125 | - | 1 | - | - | 1 | - | 2.21 | - | 4.71 | 3.97 |
| | - | 0.17 | - | 1 | - | - | 1 | - | 1.33 | - | 4.77 | 4.08 |
| | - | 0.20 | - | 1 | - | - | 1 | - | 1.18 | - | 4.66 | 3.90 |
| | - | 0.25 | - | 1 | - | - | 1.35 | - | 1 | - | 4.72 | 4.05 |
| | - | 0.50 | - | 1 | - | - | 2.77 | - | 1 | - | 4.73 | 4.09 |
| | - | 1 | - | 1 | - | - | 5.05 | - | 1 | - | 4.93 | 4.19 |
| | - | 1 | - | 2 | - | - | 3.61 | - | 1 | - | 4.95 | 4.36 |
| | - | 1 | - | 4 | - | - | 1.85 | - | 1 | - | 4.96 | 4.49 |
| NiCo-Al | - | 1 | 1 | - | - | - | 21.24 | 1 | - | - | 4.96 | 4.37 |
| NiZn-Al | - | 1 | - | - | 1 | - | 16.70 | - | - | 1 | 5.01 | 4.60 |
| CoZn-Al | - | - | 1 | - | 1 | - | - | 1 | - | 1.48 | 5.10 | 4.76 |
| CoCu-Al | - | - | 1 | 1 | - | - | - | 1 | 8.76 | - | 4.56 | 3.78 |
| CuZn-Al | - | - | - | 4 | 4 | - | - | - | 7.01 | 1 | 4.62 | 3.87 |
| NiCoCu-Al | - | 1 | 1 | 1 | - | - | 22.11 | 1 | 6.15 | - | 4.97 | 4.39 |
| NiCuZn-Al | - | 1 | - | 1 | 1 | - | 15.80 | - | 3.73 | 1 | 4.95 | 4.39 |
| NiCoZn-Al | - | 1 | 1 | - | 1 | - | 21.84 | 1 | - | 1.33 | 4.92 | 4.49 |
| CoCuZn-Al | - | - | 1 | 1 | 1 | - | - | 1 | 11.24 | 1.45 | 4.80 | 4.06 |
| NiCoCuZn-Al | - | 1 | 1 | 1 | 1 | - | 17.67 | 1 | 5.23 | 1.44 | 4.95 | 4.46 |
| MgNiCoCuZn-Al | 1 | 1 | 1 | 1 | 1 | 0.03 | 17.03 | 1 | 5.31 | 1.36 | 5.03 | 4.61 |
| MgCoCu-Al | 1 | - | 1 | 1 | - | 0.06 | - | 1 | 7.81 | - | 4.87 | 4.21 |
| MgCoZn-Al | 4 | - | 4 | - | 4 | 0.11 | - | 1 | - | 1.32 | 5.21 | 4.91 |
| MgCuZn-Al | 1 | - | - | 1 | 1 | 0.06 | - | - | 6.15 | 1 | 4.83 | 4.20 |
| MgCo-Al | 4 | - | 4 | - | - | 1 | - | 22.47 | - | - | 5.00 | 4.34 |
| MgCu-Al | 1 | - | - | 1 | - | 1 | - | - | 122.2 | - | 4.88 | 4.07 |
| MgZn-Al | 4 | - | - | - | 4 | 1 | - | - | - | 45.63 | 5.14 | 4.83 |

¹ The initial molar ratio of the aluminum was at 1 in every case.

In X-ray diffraction, no significant differences between the diffractograms of the LDHs, LTHs, and even LMHs (not shown) were found; however, the ICP analysis revealed large variations in their compositions (Table 1). The incorporation of the Ni²⁺ was about five times more favored than that of the Cu²⁺, and more than 17 and 21 times compared to the Zn²⁺ and Co²⁺, respectively. The same numbers for the incorporation of Cu²⁺, relative to that of the Zn²⁺ and Co²⁺, were 7 and 9, respectively. The ratio between the incorporated Co²⁺ and Zn²⁺ was about 1.5 when only these two metals were present during the building into the gibbsite framework. Definitely, the incorporation of the Mg²⁺ ions was the most negligible, even compared to the Zn²⁺ and Co²⁺; its amount was 20–50 times lower in the corresponding LTHs. These differences changed slightly for the LMHs due to the simultaneous and competing incorporation of more than two metal cations. These experiments were repeated in part, using perchlorate salts as starting materials. The affinity order found for perchlorate-containing systems were largely identical with those found for nitrate-containing ones (Table S1). These data led us to expand the well-known selectivity series [19] as follows:



As has been discussed elsewhere, the incorporation of the extraneous cations is mainly determined by the ionic radii and the solvation enthalpies of the metal ions [11,19]. However, the Shannon–Prewitt radius of the Mg²⁺ (72 pm) is between the values of octahedrally coordinated Ni²⁺ (69 pm) and Cu²⁺ (73 pm) ions [31]. Its hydration enthalpy (−1921 kJ/mol) is close to all of the investigated M(II) cations (for example, −1996 kJ/mol

for Co^{2+} and -2105 kJ/mol for Ni^{2+} [32]). In addition, the water solubility of the Mg^{2+} salts is also not outstandingly different from those of the other salts. Therefore, the interpretation of the lowest position of the Mg^{2+} ions and, thus, the difficulties experienced during synthesis of the $\text{MgAl}_4\text{-X}^{\text{n-}}$ -LDHs, is still not explained. It is conceivable that the answer is hiding in the water-exchange rate constants since the Mg^{2+} ion has a similar rate to that of the Co^{2+} , which are largely lower compared to the values of Zn^{2+} and Cu^{2+} [33]. However, the Ni^{2+} cations show the slowest ligand exchange, which can be compensated for by its small ionic radius (the smallest among the cations studied). The mechanism of the entry of the metal ions into the vacant octahedral holes of the aluminum trihydroxide structure is still not fully clarified: the two competing theories are the solid-state topotactic imbibition of the metal cations and dissolution–reprecipitation [11,34]). On the basis of the data shown above, the mechanism must involve a step or steps where the metal cations partially or totally lose the hydrating water molecules, the rate of which affects the efficiency of the incorporation.

3.3. Optical Properties and Morphology of the Solids

The optical properties, the coordination and oxidation state, and the energy bandgap values of the materials prepared were determined using the UV-Vis DRS technique. The spectra of the solids contain a large number of bands. In all cases (Figures S8–S12), around 230, 240 and 255 nm, the peaks were related to the oxygen-to-metal charge transfer transitions, and the band of the interlamellar nitrate anions was clearly observable at 300–310 nm [35]. As expected, for the $\text{MgAl}_4\text{-}$, $\text{ZnAl}_4\text{-}$ LDHs and $\text{MgZnAl}_8\text{-}$ LTH, there were no other adsorptions in the investigated wavenumber range (Figure S11). However, the most crowded spectra were connected to the nickel-containing solids, due to the incorporation of the Ni^{2+} , both with tetrahedral and octahedral coordination (Figures S8 and S9). The peaks at 365 and 415 nm can be ascribed to the d-d transition of the octahedral nickel cations, while the adsorption at $\sim 645 \text{ nm}$ showed the presence of nickel with tetrahedral geometry [36,37]. At around 745 nm for the copper-containing, 450 and 510 nm for the cobalt-containing solids, the spectra signified that these cations are octahedrally coordinated (Figures S8–S12) [38]. In most of the cases, the corresponding wide peaks indicate their remarkably distorted environments.

It is worthwhile discussing the situation when the synthesis of the $\text{CoAl}_4\text{-NO}_3^-$ -LDH was not successful, using a 1:1 Co:Al initial molar ratio (Figure S6). In spite of the absence of LDH reflections, the incorporation of the Co^{2+} ions commenced and, thus, the solid that was prepared had a bluish color. As opposed to the adsorption profile of the $\text{CoAl}_4\text{-NO}_3^-$ -LDH obtained at a 4:1 initial molar ratio of Co:Al, in this case, the spectrum showed the presence of tetrahedrally coordinated Co^{2+} with a broad peak from 500 to 700 nm (maxima at 625 nm, Figure S12) [39]. Although in most cases, the incorporation of the octahedral metal cations occurred, there are some examples of tetrahedral geometry in these aluminum-rich LDHs [19,40]. In addition, in our recent study, tetrahedral Ni^{2+} coordination was seen in certain NiAl_4 solids [24]. Therefore, it might be speculated that the formation of these types of $\text{Al}(\text{OH})_3$ -based LDHs commences with the insertion of the metal cations into tetrahedral geometry.

Finally, in most of these cases, the evolution of the direct and indirect optical band gaps indicated a significant redshift in the energy values, compared to the starting milled gibbsite reagent (Table 1 and Table S2). This shift was largest for the incorporation of Cu^{2+} , and was highly dependent on the number of cations. Interestingly, the incorporation of the Mg^{2+} resulted in some blue-shift relative to the values of the corresponding solids.

The morphology of the LDHs when synthesized was largely amorphous and slightly laminated, resembling that of milled gibbsite [15], but disk-like particles were observable in several cases, like those of $\text{LiAl}_2\text{-}$ LDH [41]. These features are clearly seen in $\text{ZnAl}_4\text{-}$ and $\text{MgAl}_4\text{-}$ LDHs (200–300 nm diameter and 20–40 nm width) and, to a lesser extent, in $\text{CuAl}_4\text{-}$ LDH (300–400 nm diameter and $< 100 \text{ nm}$ width) with nitrate anions (Figure 2a). For

the perchlorate-containing CuAl_4 -LDH and the nitrate-containing CoAl_4 -LDH, only the gibbsite-like morphology with significant deformation was registered (Figures 2b and S13).

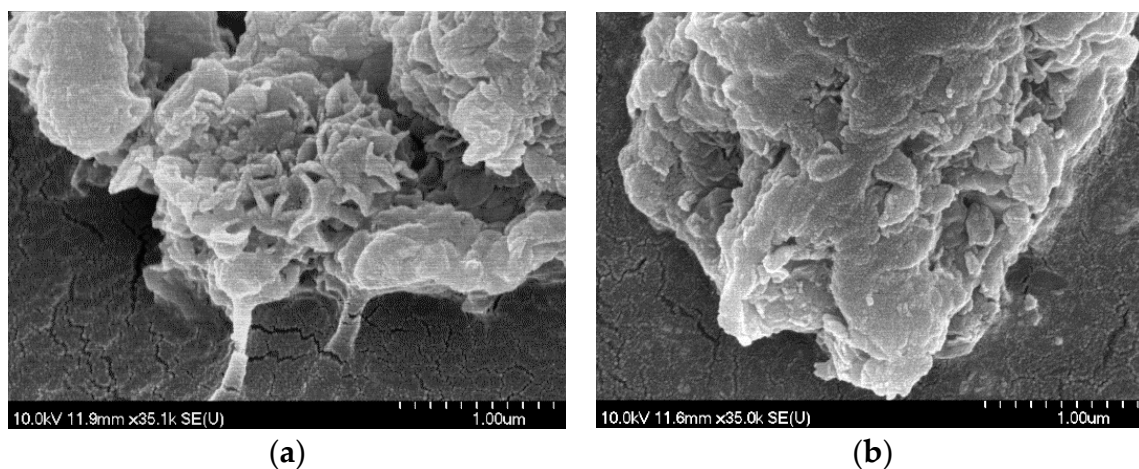


Figure 2. SEM photos of CuAl_4 -LDHs with nitrate (a) and perchlorate (b) interlayer anions.

3.4. Catalytic Oxidation of Carbon Monoxide over the Aluminum-Rich LDHs as Catalysts

The imperfect combustion of fossil fuels results mainly in the formation of the highly toxic carbon monoxide (CO) from industrial as well as personal use (engines of vehicles, gas boilers). Therefore, recently, the catalytic oxidation of CO has received considerable attention. In recent years, the focus is increasingly on its oxidation at low temperatures (below 250–300 °C) over cost-effective catalysts (substituting the generally used noble metals) [42,43]. The Al-rich LDHs are promising precursors for these catalysts: they have great potential due to the atomic distribution of the low-transition metal content in the layers. Moreover, the high aluminum content could prevent sintering of the in situ formed particles in M(0) (elemental) form [44]. In addition, the heat-induced topotactic transformation of LDHs means the retaining of their ordered layered framework even after the removal of the molecules from the interlayer space, leaving behind highly porous residues.

In this research, the main goal was to map, firstly, the catalytic feasibility of these special M(II)-poor layered double hydroxides and to investigate the influence of the temperature rising on the conversion values, regarding the structural transformations and the departure of the interlamellar spaces. Therefore, the commonly applied pre-activation (oxidation, reduction) steps had to be skipped to get a clearer picture. Relative to the performance of the milled starting gibbsite reagents, the incorporation of the extraneous metal cations could increase the conversion of the CO, and products other than CO_2 were not detected (Figure 3).

First, the $\text{M(II)Al}_4\text{-NO}_3^-$ -LDHs were tested as catalyst precursors. In the case of the zinc-containing sample, the oxidation commenced at 400 °C, while it had already begun at 300 °C for the nickel, cobalt and copper cation-containing ones. Interestingly, the $\text{MgAl}_4\text{-NO}_3^-$ -LDH precursor displayed the worst performance, but, with the exception of the milled Al(OH)_3 , all materials showed largely stable or enhancing CO transformation capabilities during the long-term activity tests. However, the cobalt- and copper-incorporated LDHs attested to higher conversion at the beginning of the process (at 300 °C); they showed some lags compared to the activity of the NiAl_4 -LDH between 350 and 550 °C.

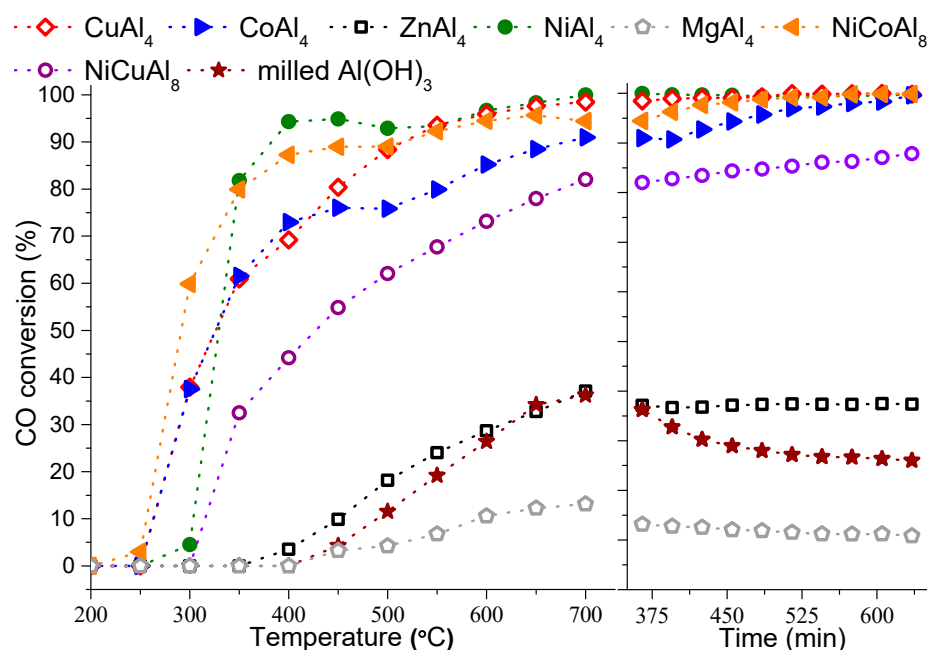


Figure 3. CO conversion values and long-term activity tests (at 700 °C) of the milled $\text{Al}(\text{OH})_3$, and the as-prepared LDHs and LTHs, at various reaction temperatures.

Therefore, the combination of the metal contents by preparing NiCuAl_8 - and NiCoAl_8 -LTHs (using the solids obtained during the syntheses with 0.20:1:1 Ni:Cu:Al and 1:21:1 Ni:Co:Al initial molar ratios) seemed like a logical step to intensify the CO transformation potential. No beneficial effect was observed in the case of the NiCuAl_8 -LTH; however, the incorporation of the cobalt cation next to the Ni(II) turned out to be useful. The CO conversion was found to increase up to ~60% from ~38% at a 300 °C reaction temperature, and CO_2 formation was already observed at 250 °C (compared to the performance of the CoAl_4 -LDH). Finally, coke formation over the catalysts was not experienced on any occasion at the end of the long term activity tests (at 700 °C, Figure S14), and the XRD measurements detected only the reflections of the spinel-like phases (according to the crystal database card of the substoichiometric nickel aluminate, JCPDS#81-0710).

Commonly, LDHs have numerous well-separated weight losses above 100/150 °C and, thus, their application in pristine form was highly limited. All LDHs showed similar thermal behavior with endothermic processes; the incorporation of nickel [24], cobalt, copper, zinc and even magnesium ions did not result in significant variations (Figure S15). The departure of the physically adsorbed water occurred between 100 and 200 °C, and the interlayer water molecules were removed generally until 300 °C. At higher temperatures, the decomposition of the interlamellar nitrate anions and the dehydroxylation of the layers took place. However, the mass losses always showed some overlap (the departure of the surface hydroxide parts and physically adsorbed water occurred partially in parallel as the evaporation of the interlamellar H_2O and the removal of the interlayered anions/structural hydroxides). The state of the catalysts was mainly the mixture of the metal oxides/hydroxides, with minimal adsorbed/intercalated water content in the temperature range of the commencement of CO oxidation (250–400 °C).

The CO chemisorption and the dehydration/dehydroxylation of the catalysts was followed by DRIFT measurements, applying 10% CO/He flow (for all samples, representative examples are shown for milled $\text{Al}(\text{OH})_3$ and NiCoAl_8 -LTH in Figure S16 and for NiAl_4 -LDH in Figure 4).

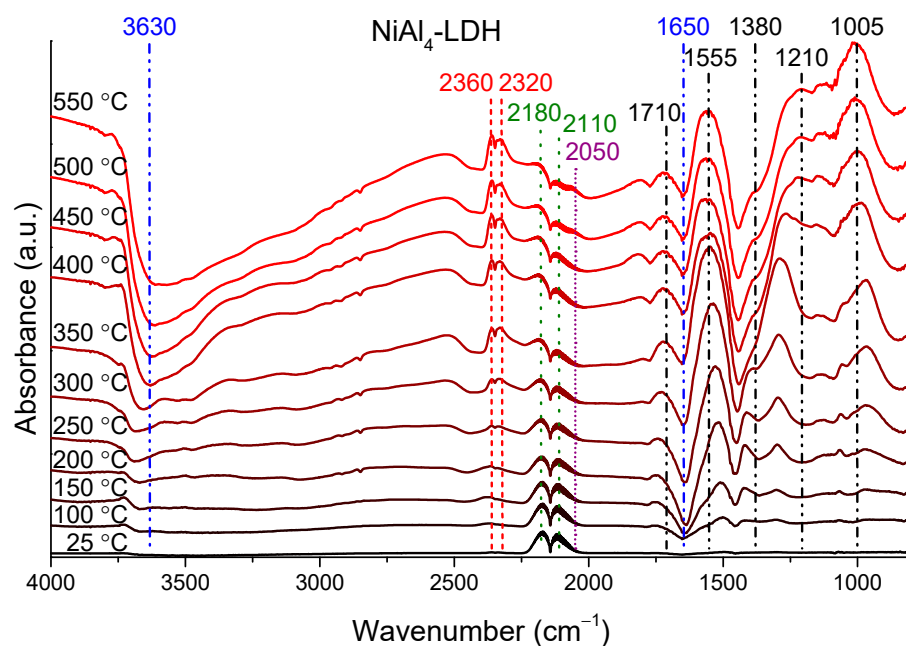


Figure 4. DRIFT spectra of the NiAl₄-LDH, heated up to 550 °C in the presence of carbon monoxide-helium flow.

The gradual decrease of the structural and crystalline water content is indicated by the growth of the negative peaks around 3500 cm⁻¹ and 1650 cm⁻¹. While the double bands in the 2370–2320 cm⁻¹ and in the 2180–2110 cm⁻¹ regions show the presence of gaseous carbon dioxide and monoxide, respectively, the peaks under 1800 cm⁻¹ wavenumber could be attributed to the different adsorbed carboxylate/carbonate/formate species formed by the reaction of the CO/CO₂ molecules and surface Al/M(II)-OH groups [45]. Due to the high sensitivity of this technique for CO₂, their formation was detectable at somewhat (50–100 °C) lower temperatures than by gas chromatography. Finally, a small shoulder (2050 cm⁻¹) next to the vibration of gaseous CO molecules appeared at higher temperatures, which can be assigned to the adsorption of CO to metallic nickel [46,47], presumably generated during the redox reaction between the Ni(II) and CO. These data demonstrate that the CO chemisorption and, thus, the oxidation process is closely related to the elemental and ionic form of the metals in the LDH/LTH phases.

4. Conclusions

Based on gibbsite modification, a novel and facile synthesis route was further developed to prepare copper-poor and aluminum-rich CuAl₄-type layered double hydroxides in phase-pure form for the first time. The chemical quality of the impregnating solution was varied, using copper bromide, chloride, nitrate and perchlorate starting salts. The formation of the expected copper hydroxide impurities could be minimized for the syntheses with bromide and chloride salts and totally eliminated when nitrate and perchlorate salts were used. The research also included the incorporation of Mg(II), Ni(II), Co(II) and Zn(II) ions and, thus, led to the preparation of layered triple and multiple hydroxides. Their composition yielded a preference order of the metals in the well-known affinity series of the incorporating cations. Compared to the Co(II), the imbibition of the Ni(II) and Cu(II) was about 21 and 9 times more favored, respectively, while this number was only around 1.5 in the case of competition with Zn(II). The last place was occupied by magnesium ions (possibly owing to their slow water-exchange rate).

The scanning electron microscopy images revealed disk-like particles. The optical analysis of the solids showed mainly the incorporation of the metal ions in octahedral form but, in a few cases, the tetrahedral coordination of the nickel and cobalt was also registered. The thermogravimetric analysis indicated thermal behavior independent from the quality

of the incorporated metal ions. The cobalt-, nickel- and copper-containing materials offered enhanced carbon monoxide oxidation performances relative to those of the starting gibbsite, ZnAl_4 - and MgAl_4 -LDHs. The catalytic tests highlighted the remarkable catalytic potential of the layered hydroxides with mixed transition metal contents.

Supplementary Materials: The following are available online at <https://www.mdpi.com/article/10.3390/ma14174880/s1>, Figure S1: XRD patterns of the $\text{CuAl}_4\text{-Cl}^-$ -LDH solids, Figure S2: XRD patterns of the $\text{CuAl}_4\text{-Br}^-$ -LDH solids, Figure S3: Infrared spectra of the CuAl_4 -LDHs, prepared with nitrate and perchlorate interlayer anions, Figure S4: X-ray diffraction traces of the $\text{NiCuAl}_4\text{-NO}_3^-$ -LTH solids with various initial Ni:Cu molar ratios, Figure S5: XRD patterns of the $\text{NiCuAl}_4\text{-NO}_3^-$ -LTH materials with different initial Ni:Cu molar ratios, Figure S6: XRD curves of the CoAl_4 - and $\text{ZnAl}_4\text{-NO}_3^-$ -LDHs with different initial Co/Zn:Al molar ratios, Figure S7: XRD patterns of the $\text{MgAl}_4\text{-NO}_3^-$ -LDH solids with various milling times and initial Mg:Al molar ratios, Figure S8: UV-Vis diffuse reflection spectra of the NiCuAl -LTHs prepared with various initial Ni:Cu molar ratios, Figure S9: UV-Vis diffuse reflection spectra of nickel-containing LTHs/LMHs, Figure S10: UV-Vis-DR spectra of copper-containing materials, Figure S11: UV-Vis diffuse reflection spectra of zinc-containing solids and the MgAl_4 -LDH; Figure S12: UV-Vis-DR spectra of cobalt-containing samples, Figure S13: SEM images of the ZnAl_4 - (A), MgAl_4 - (B) and CoAl_4 -LDH (C) prepared with nitrate interlamellar anions, Figure S14: Powder X-ray diffraction patterns of the spent catalysts after long-term carbon monoxide oxidation at 700 °C reaction temperature, Figure S15: Thermogravimetric, derivative thermogravimetric and differential thermal analysis curves of the magnesium-, cobalt-, copper- and zinc-containing LDHs prepared with nitrate interlamellar anions, Figure S16: DRIFT spectra of the milled $\text{Al}(\text{OH})_3$ and NiCoAl_8 -LTH, heated up to 550 °C in the presence of carbon monoxide–helium flow, Table S1: The molar ratios of the incorporated metal ions into the gibbsite structure, Table S2: Optical properties of the prepared LDHs.

Author Contributions: Conceptualization, M.S.; methodology, M.S., A.A.Á., Z.K. (Zsolt Kása), K.B. and R.M.; formal analysis: A.S.; investigation, M.S., A.A.Á. and K.B.; resources, A.S., Z.K. (Zoltán Kónya) and Á.K.; writing—original draft preparation, M.S.; writing—review and editing, P.S.; visualization, M.S.; supervision, P.S.; project administration, P.S.; funding acquisition, P.S. All authors have read and agreed to the published version of the manuscript.

Funding: M.S. gratefully acknowledges the support of the ÚNKP-20-4-SZTE-623 New National Excellence Program of the Ministry for the Innovation and Technology from the Source of the National Research Development and Innovation Fund. A.S. gratefully acknowledges the support of the Bolyai Janos Research Fellowship of the Hungarian Academy of Science and the “ÚNKP-20-5-SZTE-663” New National Excellence Program of the Ministry for Innovation and Technology. The financial support of the Ministry of Human Capacities through the EFOP-3.6.1-16-2016-00014 project and the 20391-3/2018/FEKUSTRAT are acknowledged. All financial help is highly appreciated.

Institutional Review Board Statement: Not applicable.

Informed Consent Statement: Not applicable.

Data Availability Statement: All the data is available within the manuscript and the electronic supplementary information.

Conflicts of Interest: The authors declare no conflict of interest.

References

1. Del Hoyo, C. Layered double hydroxides and human health: An overview. *Appl. Clay Sci.* **2007**, *36*, 103–121. [[CrossRef](#)]
2. Hafez, I.H.; Berber, M.R.; Minagawa, K.; Mori, T.; Tanaka, M. Formulation of polyacrylic acid-layered double hydroxide composite system as a soil conditioner for water management. *Int. J. Mod. Phys. Conf. Ser.* **2012**, *48*, 138–143. [[CrossRef](#)]
3. Gao, Y.; Wu, J.; Wang, Q.; Wilkie, C.A.; O'Hare, D. Flame retardant polymer/layered double hydroxide nanocomposites. *J. Mater. Chem. A* **2014**, *2*, 10996–11016. [[CrossRef](#)]
4. Szabados, M.; Ádám, A.A.; Traj, P.; Muráth, S.; Baán, K.; Béteky, P.; Kónya, Z.; Kukovecz, Á.; Sipos, P.; Pálinkó, I. Mechanochemical and wet chemical syntheses of CaIn -layered double hydroxide and its performance in a transesterification reaction compared to those of other $\text{Ca}_2\text{M}(\text{III})$ hydrocalumites (M: Al, Sc, V, Cr, Fe, Ga) and $\text{Mg}(\text{II})$ -, $\text{Ni}(\text{II})$ -, $\text{Co}(\text{II})$ - or $\text{Zn}(\text{II})$ -based hydrotalcites. *J. Catal.* **2020**, *391*, 282–297.

5. Prescott, H.A.; Li, Z.J.; Kemnitz, E.; Trunschke, A.; Deutsch, J.; Lieske, H.; Auroux, A. Application of calcined Mg–Al hydrotalcites for Michael additions: An investigation of catalytic activity and acid–base properties. *J. Catal.* **2005**, *234*, 119–130. [[CrossRef](#)]
6. Wu, M.J.; Wu, J.Z.; Zhang, J.; Chen, H.; Zhou, J.Z.; Qian, G.R.; Xu, Z.P.; Du, Z.; Rao, Q.L. A review on fabricating heterostructures from layered double hydroxides for enhanced photocatalytic activities. *Catal. Sci. Technol.* **2018**, *8*, 1207–1228. [[CrossRef](#)]
7. Evans, G.D.; Slade, R.C.T. Structural aspects of layered double hydroxides. *Struct. Bond.* **2006**, *119*, 1–87.
8. Miyata, S. Anion-exchange properties of hydrotalcite-like compounds. *Clays Clay Miner.* **1983**, *31*, 305–311. [[CrossRef](#)]
9. Forano, C.; Hibino, T.; Leroux, F.; Taviot-Gu  ho, C. Layered double hydroxides. *Dev. Clay Sci.* **2006**, *1*, 1021–1095.
10. Williams, G.R.; Dunbar, G.; Beer, A.J.; Fogg, A.M.; O’Hare, D. Intercalation chemistry of the novel layered double hydroxides [MAl₄(OH)₁₂](NO₃)₂·yH₂O (M = Zn, Cu, Ni and Co). 1: New organic intercalates and reaction mechanisms. *J. Mater. Chem.* **2006**, *16*, 1222–1230. [[CrossRef](#)]
11. Britto, S.; Kamath, P.V. Polytypism, disorder, and anion exchange properties of divalent ion (Zn, Co) containing bayerite-derived layered double hydroxides. *Inorg. Chem.* **2010**, *49*, 11370–11377. [[CrossRef](#)]
12. Gupta, S.; Agarwal, D.D.; Banerjee, S. Lithium aluminium layered double hydroxides: Synthesis and application in poly (vinyl chloride). *Int. J. Polym. Mater.* **2012**, *61*, 985–998. [[CrossRef](#)]
13. Fogg, A.M.; O’Hare, D. Study of the intercalation of lithium salt in gibbsite using time-resolved in situ X-ray diffraction. *Chem. Mater.* **1999**, *11*, 1771–1775. [[CrossRef](#)]
14. Su, L.W.; Lin, D.J.; Uan, J.Y. Novel dental resin composites containing LiAl-F layered double hydroxide (LDH) filler: Fluoride release/recharge, mechanical properties, color change, and cytotoxicity. *Dent. Mater.* **2019**, *35*, 663–672. [[CrossRef](#)]
15. Fogg, A.M.; Williams, G.R.; Chester, R.; O’Hare, D. A novel family of layered double hydroxides—[MAl₄(OH)₁₂](NO₃)₂·xH₂O (M = Co, Ni, Cu, Zn). *J. Mater. Chem.* **2004**, *14*, 2369–2371. [[CrossRef](#)]
16. Chitrakar, R.; Makita, Y.; Sonoda, A.; Hirotsu, T. Synthesis of a novel layered double hydroxides [MgAl₄(OH)₁₂](Cl)₂·2.4H₂O and its anion-exchange properties. *J. Hazard. Mater.* **2011**, *185*, 1435–1439. [[CrossRef](#)] [[PubMed](#)]
17. Rees, J.R.; Burden, C.S.; Fogg, A.M. New layered double hydroxides by prepared by the intercalation of gibbsite. *J. Solid State Chem.* **2015**, *224*, 36–39. [[CrossRef](#)]
18. Pushparaj, S.S.C.; Jensen, N.D.; Forano, C.; Rees, G.J.; Prevot, V.; Hanna, J.V.; Ravnsb  k, D.B.; Bjerring, M.; Nielsen, U.G. Structural investigation of Zn(II) insertion in bayerite, an aluminum hydroxide. *Inorg. Chem.* **2016**, *55*, 9306–9315. [[CrossRef](#)]
19. Williams, G.R.; Moorhous, S.J.; Prior, T.J.; Fogg, A.M.; Rees, N.H.; O’Hare, D. New insights into the intercalation chemistry of Al(OH)₃. *Dalton Trans.* **2011**, *40*, 6012–6022. [[CrossRef](#)]
20. Jensen, N.D.; Duong, N.T.; Bolanz, R.; Nishiyama, Y.; Rasmussen, C.A.; Gottlicher, J.; Steininger, R.; Prevot, V.; Nielsen, U.G. Synthesis and structural characterization of a pure ZnAl₄(OH)₁₂(SO₄)₂·2.6H₂O layered double hydroxide. *Inorg. Chem.* **2019**, *58*, 6114–6122. [[CrossRef](#)]
21. Isupov, V.P. Intercalation compound of aluminium hydroxide. *J. Struct. Chem.* **1999**, *40*, 672–685. [[CrossRef](#)]
22. Barnard, B.A.; Labuschagn  , F.J.W.J. Exploring the wet mechanochemical synthesis of Mg–Al, Ca–Al, Zn–Al and Cu–Al layered double hydroxides from oxides, hydroxides and basic carbonates. *Crystals* **2020**, *10*, 954. [[CrossRef](#)]
23. Ferencz, Z.; Szabados, M.; Adok-Sipiczki, M.; Kukovecz, A.; Konya, Z.; Sipos, P.; Palinko, I. Mechanochemical assisted synthesis of pristine Ca(II)Sn(IV)-layered double hydroxides and their amino acid intercalated composites. *Mater. Sci.* **2014**, *49*, 8479–8486. [[CrossRef](#)]
24. Szabados, M.; Szabados, T.; Mucsi, R.; Ba  n, K.; S  pi, A.; K  nya, Z.; Kukovecz,   .; P  link  , I.; Sipos, P. Mechanochemically induced gibbsite intercalation for preparing NiAl₄-layered double hydroxides with interlayer halide and oxoanions (Cl[−], Br[−], I[−], NO₃[−], NH₂SO₃[−], SO₄^{2−}, ClO₄[−]) and their application in CO₂ methanation reaction. *J. Colloid Interface Sci.* **2021**. submitted.
25. Bal  z, P. *Mechanochemistry in Nanoscience and Minerals Engineering*; Springer: Berlin/Heidelberg, Germany, 2008; pp. 111–114.
26. Huang, L.; Wang, J.; Gao, Y.; Qiao, Y.; Zheng, Q.; Gou, Z.; Zhao, Y.; O’Hare, D.; Wang, Q. Synthesis of LiAl₂-layered double hydroxides for CO₂ capture over a wide temperature range. *J. Mater. Chem. A* **2014**, *2*, 18454–18462. [[CrossRef](#)]
27. Britto, S.; Kamath, P.V. Synthesis, structure refinement and chromate sorption characteristics of an Al-rich bayerite-based layered double hydroxide. *J. Solid State Chem.* **2014**, *215*, 206–210. [[CrossRef](#)]
28. Klopogge, J.T.; Ruan, H.D.; Frost, R.L. Thermal decomposition of bauxite minerals: Infrared emission spectroscopy of gibbsite, boehmite and diaspore. *J. Mater. Sci.* **2002**, *37*, 1121–1129. [[CrossRef](#)]
29. Song, J.; Leng, M.; Fu, X.; Liu, J. Synthesis and characterization of nanosized zinc aluminate spinel from a novel Zn–Al layered double hydroxide precursor. *J. Alloy. Compd.* **2012**, *543*, 142–146. [[CrossRef](#)]
30. Miyata, S. The syntheses of hydrotalcite-like compounds and their structures and physico-chemical properties I: The systems Mg²⁺–Al³⁺–NO₃[−], Mg²⁺–Al³⁺–Cl[−], Mg²⁺–Al³⁺–ClO₄[−], Ni²⁺–Al³⁺–Cl[−] and Zn²⁺–Al³⁺–Cl[−]. *Clay Clay Miner.* **1975**, *23*, 369–375. [[CrossRef](#)]
31. Shannon, R.D. Revised effective ionic radii and systematic studies of interatomic distances in halides and chalcogenides. *Acta Cryst.* **1976**, *A32*, 751–767. [[CrossRef](#)]
32. Smith, D.W. Ionic hydration enthalpies. *J. Chem. Educ.* **1977**, *54*, 540–542. [[CrossRef](#)]
33. Lincoln, S.F. Mechanistic studies of metal aqua ions: A semi-historical perspective. *Helv. Chim. Acta* **2005**, *88*, 523–545. [[CrossRef](#)]
34. Graham, R.T.; Hu, J.Z.; Zhang, X.; Dembowski, M.; Jaegers, N.R.; Wan, C.; Bowden, M.; Lipton, A.S.; Felmy, R.A.; Clark, S.B.; et al. Unraveling gibbsite transformation pathways into LiAl-LDH in concentrated lithium hydroxide. *Inorg. Chem. A* **2019**, *58*, 12385–12394. [[CrossRef](#)]

35. Kim, H.; Lee, B.I.; Jeong, H.; Byeon, S.H. Relationship between interlayer anions and photoluminescence of layered rare earth hydroxides. *J. Mater. Chem. C* **2015**, *3*, 7437–7445. [[CrossRef](#)]
36. Lorenzi, G.; Baldi, G.; Di Benedetto, F.; Faso, V.; Lattanzi, P.; Romanelli, M. Spectroscopic study of a Ni-bearing gahnite pigment. *J. Eur. Ceram. Soc.* **2006**, *26*, 317–321. [[CrossRef](#)]
37. Jiménez-González, C.; Boukha, Z.; de Rivas, J.J.; Delgado, M.Á.; González-Velasco, J.R.; Gutiérrez-Ortiz, J.I.; López-Fonseca, R. Structural characterisation of Ni/alumina reforming catalysts activated at high temperatures. *Appl. Catal. A Gen.* **2013**, *466*, 9–20. [[CrossRef](#)]
38. Velu, S.; Suzuki, K.; Hashimoto, S.; Satoh, N.; Ohashi, F.; Tomura, S. The effect of cobalt on the structural properties and reducibility of CuCoZnAl layered double hydroxides and their thermally derived mixed oxides. *J. Mater. Chem.* **2001**, *11*, 2049–2060. [[CrossRef](#)]
39. Dondi, M.; Ardit, M.; Cruciani, G.; Zanelli, C. Tetrahedrally coordinated Co²⁺ in oxides and silicates: Effect of local environment on optical properties. *Am. Mineral.* **2014**, *99*, 1736–1745. [[CrossRef](#)]
40. Besserguenev, A.V.; Frogg, A.M.; Francis, R.J.; Price, S.J.; O'Hare, D. Synthesis and structure of the gibbsite intercalation compounds [LiAl₂(OH)₆]X [X = Cl, Br, NO₃] and [LiAl₂(OH)₆]Cl·H₂O using synchrotron X-ray and neutron powder diffraction. *Chem. Mater.* **1997**, *9*, 241–247. [[CrossRef](#)]
41. Qu, J.; Li, X.; Lei, Z.; Li, Z.; Chen, M.; Zhang, Q. Mechano-hydrothermal synthesis of tetraborate pillared Li–Al layered double hydroxides. *J. Am. Ceram. Soc.* **2016**, *99*, 1151–1154. [[CrossRef](#)]
42. Ramesh, K.; Chen, L.; Chen, F.; Liu, Y.; Whang, Z.; Han, Y.F. Re-investigating the CO oxidation mechanism over unsupported MnO, Mn₂O₃ and MnO₂ catalysts. *Catal. Today* **2008**, *131*, 477–482. [[CrossRef](#)]
43. Soubaihi, R.M.A.; Saoud, K.M.; Dutta, J. Critical review of low-temperature CO oxidation and hysteresis phenomenon on heterogeneous catalysts. *Catalysts* **2018**, *8*, 660. [[CrossRef](#)]
44. Gabrovska, M.; Edreva-Kardjieva, R.; Crişan, D.; Tzvetkov, P.; Shopska, M.; Shtereva, I. Ni–Al layered double hydroxides as catalyst precursors for CO₂ removal by methanation. *React. Kinet. Mech. Cat.* **2012**, *105*, 79–99. [[CrossRef](#)]
45. Subramanian, N.D.; Kumar, C.S.S.R.; Watanabe, K.; Fischer, P.; Tanaka, R.; Spivey, J.L. A DRIFTS study of CO adsorption and hydrogenation on Cu-based core–shell nanoparticles. *Catal. Sci. Technol.* **2012**, *2*, 621–631. [[CrossRef](#)]
46. Kitla, A.; Safonova, O.V.; Föttinger, K. Infrared studies on bimetallic copper/nickel catalysts supported on zirconia and ceria/zirconia. *Catal. Lett.* **2013**, *143*, 517–530. [[CrossRef](#)] [[PubMed](#)]
47. Németh, M.; Srankó, D.; Károlyi, J.; Somodi, F.; Schay, Z.; Sáfrán, G.; Sajó, I.; Horváth, A. Na-promoted Ni/ZrO₂ dry reforming catalyst with high efficiency: Details of Na₂O–ZrO₂–Ni interaction controlling activity and coke formation. *Catal. Sci. Technol.* **2017**, *7*, 5386–5401. [[CrossRef](#)]